An Investigation of the Flame Structures and Burning Speeds of H_2/CO/Air Mixtures

A Thesis presented

by

Alden William Ahlholm

to

The Department of Mechanical and Industrial Engineering

In partial fulfillment of the requirements

for the degree of

Master of Science

in

Mechanical Engineering

in the field of

Thermo-fluids

Northeastern University

Boston, Massachusetts

April 2015

ABSTRACT

With the potential of synthetic gas to be used as a replacement for natural gas in the gas turbine industry the knowledge of its fundamental thermo-physical properties is of utmost importance. The laminar burning speed and flame structures of spherically expanding flames of hydrogen and carbon monoxide mixtures (Syngas) with air have been studied over a wide range of equivalence ratios, initial mixture temperatures, and initial pressures. The mixtures studied consisted of 0.1:0.9 hydrogen to carbon monoxide ratio at initial temperatures of 298 K and 380 K, and initial pressures of 0.5 atm, 1 atm, and 2 atm. The range of equivalence ratios tested were 0.6, 1, 2, 3, and 5. Based on these initial conditions burning speed was calculated for temperatures ranging from 310-520 K at pressures between 0.5-3 atmospheres. All experimentation was conducted in a constant volume cylindrical vessel fitted in a Schlieren shadowgraph system. The shadowgraph system was used to study the structures of the flames and to understand the transition from smooth flames to cellular flames to illustrate the onset of turbulence. Pressure-time data was obtained during the combustion event through pressure transducers on the combustion chamber wall and were a primary input into the thermodynamic model used to determine the laminar burning speed. The results for the burning speed of H_2/CO/Air mixtures at the aforementioned test conditions have been compared with the results obtained by other research groups: the results agree within 7% which is within the margin of error for this experimentation.

ACKNOLEDGEMENTS

I would like to extend many thanks to Professor Hameed Metghalchi for bringing me through my time at Northeastern. Without your guidance and assistance I wouldn't be where I am today. I would also like to thank the lab team and the code architects for all the effort put into this research and the help offered to me; Omid Askari, Ali Moghaddas, Bander Alhazmi, Abdulsatar Aljanabi, and Emad Rokni. I would like to thank Kevin McCue and John Doughty for answering any questions I had.

Additionally, thank you to my parents Beth and Vincent Ahlholm for affording me the opportunity to attend Northeastern and also for always being there for me to provide support and motivation. Lastly I would like to thank Kiana Ocean for being my rock throughout this journey, I certainly could not have done it without you.

TABLE OF CONTENTS

1 Introduction 1
1.1 Background 1
1.2 Experimental Determination of Burning Speed 2
1.3 H_2/CO/Air Mixtures 5
2 Testing Methods and Experimental Facility 6
2.1 Cylindrical Combustion Chamber 6
2.2 Gas Delivery System 6
2.3 Heating System 7
2.4 Temperature Verification 7
2.5 Ignition System 8
2.6 Shadowgraph System 9
2.7 Experimental Procedure 9
2.8 Experimental Error 10
3 Burning Speed Model 12
4 Results 15
4.1 Flame Structure 15
4.2 Stretch 15
4.3 Conditions Tested 16
4.4 Data Processing 17
4.5 Laminar Burning Speed Results 18
4.6 Comparison with Previous Work 19
5 Conclusions and Future Work 20
5.1 Future Work 20
6 Appendices 21
6.1 Figures 21
6.2 Tables 40
7 References 41

LIST OF FIGURES

Figure 1: Cylindrical Chamber Profile 21
Figure 2: Cylindrical Chamber Face 21
Figure 3: Band Heaters 22
Figure 4: Gas Delivery System 22
Figure 5: Pressure Gauges 23
Figure 6: Electrical Schematic for Heating System 23
Figure 7: DP -7000 Controllers for Heaters 24
Figure 8: Temperature Correlation Plot 24
Figure 9: Extended Length Spark Plugs 25
Figure 10: Shadow Graph System Schematic 25
Figure 11: Shadow Graph System Lab Setup 26
Figure 12: Diagram of Separate States of Gas During Combustion 27
Figure 13: Flame Stability at Initial Temperature, Pressure, and 3 Equivalence Ratios 28
Figure 14: Fully Cellular flame prior to radius=4cm 29
Figure 15(L) Phi=0.6 isentrope plot for Ti=298, 350, and 380 K (R): Phi=0.6 Laminar Burning Speed vs. Stretch for Ti=298, 350, and 380K 30
Figure 16: Phi=3.0 isentrope plot for Ti =298, 350, and 380 K (R): Phi=3.0 Laminar Burning Speed vs. Stretch for Ti =298, 350 30
Figure 17: Pressure Time Experimental Data 31
Figure 18: Raw Pressure v. Time data compared to processed 'smooth' data 32
Figure 19: Laminar Burning Speed vs. Temperature T_i = 298 P_i=0.5atm 33
Figure 20: Laminar Burning Speed vs. Temperature T_i = 298 P_i=1.0atm 34
Figure 21: Laminar Burning Speed vs. Temperature T_i = 298 P_i=2.0atm 35
Figure 22: Laminar Burning Speed vs. Temperature T_i = 380 P_i=0.5 atm 36
Figure 23: Laminar Burning Speed vs. Temperature T_i = 380 P_i=1.0 atm 37
Figure 24: Laminar Burning Speed vs. Temperature T_i= 380 P_i=2.0 atm 38
Figure 25: Comparison with literature at atmospheric pressure, To=298 and various equivalence ratios 39

LIST OF TABLES

Table 1: Gas Temperature Correlation 21

1 Introduction

In this section, an overview of laminar burning speed and its importance to the combustion community is given alongside a brief review of the methods of determination of this thermos-physical property. Additionally a slight overview of synthetic gas is also presented to illustrate the need for this research.

1.1 Background

The burning speed of homogeneous gaseous fuels and diluent mixtures is critically important for the development of chemical kinetic and fluid dynamic models studying fuel oxidation both of which directly impact everyday applications involving fuel use in engines, power plants, and chemical processors. The study of laminar burning speed at high temperatures and pressures is of utmost importance for predicting and analyzing the performance of internal combustion engines and power plants in the continuing effort to reduce emissions and improve overall efficiency. As new fuels are continually developed there is a need to determine the chemical reaction mechanisms and the laminar burning speed is a pivotal tool in calibrating and validating many of these mechanisms.

Laminar burning speed is a thermo-physical property that is the direct measure of the rate of energy released during the combustion process of any combustible mixture and is a direct function of initial mixture pressure, temperature, and composition. Physically laminar burning speed is the rate of expansion of a planar, one dimensional, adiabatic flame front during combustion. Laminar burning speed is a primary input alongside adiabatic flame temperature for many turbulent combustion and wall quenching models [1-3]. Quench models determine the size of quench layers

which are the predominant source of unburned hydrocarbons in internal combustion engines, thus a key source in the formation of pollutants.

1.2 Experimental Determination of Burning Speed

The two primary methods for determining burning speed in general are based on flame type; stationary flame methods and propagating flame methods. This section will serve to provide an overview of the two most widely used methods, although it is not intended to be a complete analysis for the various methods employed by different researchers. Linnett [4], Andrews [5], and Rallis [6] have conducted thorough reviews of past measurement methods of laminar burning speed.

Stationary flame methods encompass flat flame burners, stagnation flames, and nozzle methods. With flat flame burners a stream of fuel flows into the stationary flame so the rate at which the unburned fuel enters the flame is equal to the laminar burning speed of the gas. A key drawback of the flat flame burners is a lack of consistency in the results of burning speed data depending on the location in the flame. Additionally energy losses to the burner itself reduces the overall accuracy of the flat flame method. In light of the reduced accuracy research groups such as Botha and Spalding have develop still flat flame methods that use slight variations in an attempt to circumvent the notable energy losses [7]. By stabilizing the flame with a porous plug the researchers were able to record the temperature rise of the cover at multiple fuel flow rates. They then extrapolated the ratio of volumetric flow rate to the flame disc area to determine the adiabatic flame temperature.

Nozzle stationary flame methods utilize Bunsen burner type flames that are conical in shape and experience largely the same drawbacks of its flat flame burner counterpart. In the analysis of the conical flames the velocity component normal to the flame surface gives the burning speed at that

particular location. Yet several distinct drawbacks of the conical flame method lie within the geometry of the flame. The conical flame cannot always live up to its assumed characteristics. And as a result, the primary challenge is to determine the true geometry of the flame. Researchers such as Linteris utilize conical flame methods yet they experience considerable stretch effects and it was recommended that for future work the experiment be redesigned in such a way that stretch effects could be taken into consideration [8].

The final stationary flame method to determine burning speed is the stagnation flame method also known as the counter flow method, developed by Wu and Law [9], and used most notably by Egolfopoulos [10]. This method consists of directing two identical flows of premixed combustible fuel normal to each other, with an ignition source at the flows point of contact. After ignition two flames are generated parallel on either side of the stagnation plane generated by the impinging streams of fuel. A primary drawback of the counter flow method is the oftentimes inaccurate determination of velocity profiles which are determined numerically by extrapolating the point of zero gradient.

The two primary experimental methods which use propagating flames are the flame tube method and the propagating spherical flame method. The flame tube method was developed by Chatlier [11] and consists of a cylindrical tube filled with a combustible mixture. The flame is studied using a camera to capture frames at a known rate. This rate is then used in conjunction with the images taken to determine the flames speed. A primary assumption in the flame tube method is that the flame velocity is constant across any given tube cross section, yet this has been found to be a source of error. In practice the flame tube method suffers from quenching which is significant energy loss from the flame to the wall of the tube, thus slowing the reported burning speed at the walls. Additionally the experiment is affected by gravity. The reported changes in burning speed

depend on the location of ignition in the tube (e.g. was the mixture ignited from the top of bottom of the chamber)

The propagating spherical flame method can be broken into two subcategories; constant volume and constant pressure. The method of constant pressure propagating flames was developed by Metghalchi and Eisazadeh-Far [12]. This setup uses a shadowgraph system. During the beginning stage of combustion, where pressure is assumed to be constant and all species are still in local thermodynamic equilibrium, this system is able to capture the ignition event and persist through the duration of combustion. Additionally, at the onset of ignition, the flame kernel is a constant mass system and is perfectly spherical. The model includes losses due to radiation from plasma to the surroundings, energy loss associated with the ignition source voltage drops and conduction losses to thermal boundary layers around the electrodes. The inputs to this model are flame radius as a function of time which is captured through the use of the shadowgraph system.

Constant volume propagating flame methods were used by Takizawa [13], and utilize a thermodynamic model which calls for the input of the pressure rise during combustion. The pressure data was used to determine the burned gas mass fraction. Subsequently, the laminar burning speed was calculated, this method was first developed by Lewis and Von Elbe [14]. Also in this category is a similar method developed by Metghalchi and Keck [15-16]. This method also utilizes a constant volume chamber where the pressure history over the combustion event is recorded. A model is used that assumes that all unburned gasses compress isentropically and that the burned gases are in local equilibrium. The burning speed is derived from the rate of change of the mass fraction of burned gases. The distinct advantage of the propagating flame methods is that it prevents the need for extrapolation, and that many data points can be collected along an isentrope in a single isentrope.

1.3 H_2/CO/Air Mixtures

Synthetic gas also known as syngas is the name of a combustible mixture predominantly containing varying levels of hydrogen and carbon monoxide and in some instances some levels of CO_2, CH_4, N_2, and H_2O and other higher order hydrocarbons. Syngas can be produced through the gasification of coal emissions, waste emissions to energy gasification, steam reforming of coke, and the gasification of biomass. This gas is considered an alternative fuel which is used to produce a wide range of synthetic materials, solvents, and fertilizers. Recently a large focus has been cast on this fuel for its potential use in the gas turbine industry as a replacement of natural gas. [17-20]. Thus it is of utmost importance to study and determine the fundamental combustion characteristics of the fuel to fully understand how it behaves over a wide range of combustion conditions.

2 Testing Methods and Experimental Facility

In this section both the equipment used for all data collection and the way each experiment was conducted is discussed thoroughly. This will serve to highlight the most critical components of the facility and to illustrate the step by step procedure for experimentation.

2.1 Cylindrical Combustion Chamber

The testing chamber used in this experimentation is the cylindrical vessel seen in Figures 1 and 2. The chamber has an inner diameter of 13.5cm and a length of 13cm and is made of 316 stainless steel. To complete the enclosure the ends are capped with two 3.5cm thick Pyrex windows which allow the chamber to operate to a maximum pressure of 50 atmospheres. The sole purpose of the windows is to provide a clear viewing angle through the vessel such that the chamber can be aligned in a shadowgraph setup. The shadow graph setup will be described in more detail in a later section, but the primary purpose is to allow for the recording of the combustion process. The chamber is heated using two band heaters attached on either end of the cylinder which are capable of heating the chamber upwards of 500 K highlighted in Figure 3. The temperature limit of 500 K is imposed by the material properties of the o-rings used to seal the windows to the ends of the chamber. Pressure data is acquired through the use of a Kistler 603B1 pressure transducer connected to a Kistler 5010B charge amplifier which converts the 4-20 mA signal from the transducer into a 10mV/PSIa signal which is relayed to the analog to Digital conversion box in order to record the pressure change at the wall during combustion.

2.2 Gas Delivery System

The cylindrical chamber is connected to a gas manifold as seen in Figure 4 which is the distribution system for each component of the syngas as well as providing a common piping to the vacuum

pump. Four pressure gauges are used during the filling procedure shown in Figure 5. The first is a thermocouple gauge which measures low vacuum levels and is used to determine when the chamber is sufficiently evacuated (typically around 100 millitorr). The other three gauges are piezoelectric pressure transducers and have various operation ranges; 0-15psi, 0-30psi, and 0-50 psi respectively. The pressure gauge with the range closest to the desired initial pressure of testing mixture is used to fill each component in the chamber. The vacuum pump is used to evacuate the chamber and lines not only between tests but also between each individual component added to the chamber to ensure a known quantity of each specific gas in the mixture during each test. The driving force behind the filling procedures is the method of partial pressures and it is controlled by the series of valves and transducers shown in Figure 4.

2.3 Heating System

The cylindrical vessel can be heated to 500K in order to run high temperature experiments. To heat the chamber two 1.5 kW band heaters are mounted to the flanges which hold the glass windows in place on either end of the chamber as can be seen in Figure 3. The walls of the cylinder are wrapped tightly with two layers of ½" ceramic insulation which is able to withstand upwards of 800F. The electrical schematics for the heating system can be seen in Figure 6. To control each heater an Omega DP-7000 controller was used. The DP-7000 series are on-off controllers shown in Figure 7 which meant the chamber experienced heating cycles instead of a constant temperature which will be discussed in depth in the following section.

2.4 Temperature Verification

Laminar burning speed is a strong function of temperature, thus it is pivotal that the temperature of the combustible mixture is known precisely. Due to system limitations it is impractical to measure the temperature of the gas constantly while maintaining the vacuum tight requirement for

our filling method. In lieu of these challenges a correlation between chamber surface temperature and gas temperature at each testing temperature set point was developed. The correlation was developed over three heating cycles using a thermocouple suspended in the center of the chamber, and another on the surface of the chamber in the same axial location as the internally suspended thermocouple. The two thermocouples recorded values over three heating cycles and temperature points were taken every 15 seconds. This procedure was completed for each temperature set point where testing was conducted. An example for this correlation can be seen in Figure 8, and the results of the correlation are presented in the table 1 for the three temperature levels.

Additional considerations were taken for the increase in gas temperature during the filling process due to the rapid expansion of the gas as it enters the chamber. In testing it was found that after filling the chamber with the prescribed amount of fuel allowing the mixture to stand for two minutes was adequate for the temperature of the gas to fall back to its expected value.

2.5 Ignition System

The ignition system used for the cylindrical chamber consists of a power supply, a transformer circuit, and two extended length spark plugs. In order to modify the spark plugs the built in ground was filed off and a .4mm diameter stainless steel wire was welded to the center of each sparkplug as seen in Figure 9. The modified electrodes were threaded into the chamber and the tips were separated by about 1mm at the center of the chamber as can be seen in Figure 2. The power supply is powered by AC power which is then isolated by the transformer to ensure that no erroneous voltage damages the equipment or causes premature ignition. The power supply is then converted from AC to DC and is used to charge a capacitor to the prescribed set point. Once the trigger is initialized in lab-view the capacitor is connected to ground and the DC pulse is sent to another

transformer circuit which is then converted via mutual inductance to about 3000V. After which a spark is generated at the tip of the electrodes, causing ignition.

2.6 Shadowgraph System

A shadowgraph system has been employed with the cylindrical chamber to capture the flame structure and propagation during combustion and is illustrated in Figures 10 and 11. The light source for the shadowgraph system is a 10-W Halogen lamp with a condensing lens which is placed behind a 0.3mm pin hole. The pinpoint of light leaving the lamp is captured by a spherical mirror 154.2 cm away which then reflects the light in a 15.24cm diameter circular beam which travels through the cylindrical vessel to second spherical mirror placed on the opposite end of the chamber. After the light has hit the second mirror it is again focused into a pin point 152.4 cm away into a high speed camera. The camera used is a high speed CMOS (HG-LE Redlake) which can capture 40,000 frames per second. The camera is triggered by the same program which triggers the ignition to ensure the entire combustion process is captured from the inception of the spark to the flames striking the wall.

2.7 Experimental Procedure

To begin testing the combustion chamber and gas manifold must be evacuated using the pump. After a sufficiently low pressure (ideally less than 100 millitorr) has been achieved the gas manifold system is then used to fill the chamber to the desired pressure of each specific component; hydrogen, air, and carbon monoxide. The pressure of each component, or each constituent's partial pressure is determined through the use of a spread sheet that takes into account variables such as the pressure transducers zero offset, the fuel to air ratio, and percent of hydrogen. The gases are filled by order of ascending partial pressures which changes depending on the tests initial conditions. The first component is filled using the gas manifold, once the desired pressure of the

first gas is reached the valve to the combustion chamber is closed and the lines within the manifold system are yet again evacuated to 100 millitorr. The valve for the second component of the mixture is opened and once the pressure in the line exceeds twice the pressure of the previous component of the mixture already in the chamber, the valve to the vessel is reopened allowing for the second mixture to flow into the chamber without experiencing any backflow, improving overall accuracy. This process is repeated for the number of constituents present in the combustible mixture. For syngas testing there was a total of three components. Once the chamber has been filled, the mixture is left to sit for several minutes, which as discussed in the temperature section, allows for the temperature of the mixture to fall back to its expected correlated value. Additionally this downtime allows for the mixture to become quiescent.

Burning speed measurements were restricted to flames with radii larger than 4cm, which is a size deemed large enough for stretch effects to be negligible. Measurements can only be conducted for when the flame is larger than 8cm in diameter and prior to when it reaches the outer wall of the chamber, during which time the pressure method can be used to calculate the burning speed. The high speed camera and shadowgraph system are used to verify flame symmetry, stability, and structure during each test.

2.8 Experimental Error

There are several sources of error within this experimentation and the following error analysis was outlined by Casey Bennet [20]. Initially the small rounding errors in the calculation of the mole fractions are compounded by converting the partial pressure into the expected pressure transducer value, resulting in a total error of about 1%. When filling the chamber the human error is about +/- 0.01 on each respective pressure transducer. Depending on the transducer being used, this variance can cause as much as a 0.5% error in the pressure value. A large source of error, approximately

2%, stems from the signal amplification and analog to digital conversion of the pressure signal. The largest source of error is generated when filtering the noise from the pressure signal which can range anywhere from 2%-5%. Other sources of error result from small leaks that exist in the system even when the chamber is vacuum tight. A compilation of these errors could exceed a 7% error, which illustrates the need for careful and consistent testing procedures.

3 Burning Speed Model

The model employed to calculate the burning speed based on the pressure rise inside the combustion chamber is based on a code developed by Metghalchi and Keck [15][16] that has since been modified to include several correction factors for radiative energy loss to the chamber walls, energy loss to the spark electrodes, and the temperature gradient in the preheat zone by Eisazadeh-Far et al [12]. The fundamental assumption in this model is that the combustion chamber can be broken into two primary parts consisting of burned and unburned gasses both of which behave as ideal gasses that are separated by a reaction layer which has zero thickness. The burned gas inside the reaction layer is divided into 'n' number of shells where 'n' is directly proportional to the duration of the combustion event. Each shell has a distinct independent temperature that may differ from that of the surrounding shells, yet the burned gas remains in chemical equilibrium. Working outward in Figure 12 beyond the reaction layer there exists a small preheat zone of thickness δ_{ph} which consists of unburned gas at a higher temperature than the far field unburned gas due to energy transfer from the reaction layer. Beyond the preheat layer and unburned gas there exists a boundary layer (δ_{bl}) which separates the unburned gas from the wall. Further assumptions include that both the burned and unburned gasses always behave as ideal gasses, both gasses compress isentropicly, the composition of the unburned gas is constant, and the heat flux in the burned gas is negligible.

For spherical flames the pressure time data can be used to determine the temperature distribution (T(r,t)) and the burned gas mass fraction (x_b) using the conservation of mass and energy equations along with the assumed ideal gas behavior. The conservation of mass equation used is presented in equation 1 where m is the mass of the gas in the combustion chamber, m_b is the burned gas

mass, mu is the unburned gas mass, V_c is the volume of the combustion chamber, V_e is the electrode volume, and the subscript i denotes initial conditions. Subscripts b and u represent burned and unburned components of the fuel respectively.

$$m = m_b + m_u = \frac{p_i(V_c - V_e)}{RT_i} \qquad (1)$$

The total volume of gas in the chamber is calculated using equation 2 where the subscripts follow the same naming convention.

$$V_i = V_c - V_e = V_b + V_u \qquad (2)$$

The conservation of energy equation used is presented in equation 3, where E_i is the initial energy of the unburned gas, Q_w is the conduction energy loss to the wall, Q_e is the conduction energy loss to the electrodes, Q_r is the energy loss due to radiation from the burned gas.

$$E_i - Q_e - Q_w - Q_r = E_b + E_u \qquad (3)$$

Employing the assumptions described by Eisazadeh-Far et al. [12] the mass and energy balances become equations 4 and 5 respectively where $v_i=V_i/m$ and $e_i=E_i/m$ are the initial specific volume and energy of the unburned gas in combustion vessel, v_u is the specific volume of the unburned gas. V_w, V_o, and V_e are all displacement volumes of the wall boundary layer (subscript w), preheat zone (subscript p), and the electrode boundary layer (e). Coefficients e_b and e_u are the specific energy of the burned and unburned gasses respectively, and the remaining undefined coefficients γ_b and γ_u are the specific heat ratios of again the burned and unburned gasses.

$$\int_0^{x_b} (v_b - v_u)dx = v_i - v_u + \frac{V_e + V_w + V_p}{m} \qquad (4)$$

$$\int_0^{x_b} (e_b - e_u)dx = e_i - e_u + \frac{\frac{PV_p}{\gamma_b - 1} + \frac{PV_e}{\gamma_b - 1} + \frac{PV_w}{\gamma_b - 1} - Q_r}{m} \qquad (5)$$

The preceding equations are solved using the pressure time data obtained during the combustion event for the two unknown values of burned gas mass fraction (γ_b) and radial temperature distribution through the chamber. The final result of the computation is the ability to determine the burning speed (S_u) which is illustrated in equation 6, where A_b is the surface area of a sphere the size of the burned gases within the chamber.

$$S_u = \frac{\dot{m_b}}{\rho_u A_b} = \frac{m\dot{x_b}}{\rho_u A_b} \tag{6}$$

The solution procedure is illustrated clearly by Eisazadeh-Far et al [12] and more details of the burning model can be found in several other publications by Eisazadeh, Moghaddas, and Metghalchi.[12,20-22]

4 Results

In this section the conditions tested, the methodology used to process the data, the results and their comparison to previous works are discussed. The topic of stretch is discussed along with its impact on the reported laminar burning speed.

4.1 Flame Structure

The transition to cellularity is determined by inspection of the images captured by the high speed camera during combustion. Three examples of flame structure through a combustion event are given at three conditions; p_i=1atm T_i=298 and φ=0.6, 2, and 5 in Figure 13. From Figure 13 it is clear that when φ=0.6 the flame is smooth throughout the duration of the combustion event until it strikes the wall in frame 212, this is the point where we trim our data for processing. For φ=2 we see that cellularity or turbulence occurs prior to the flame hitting the wall in frame 42, for these situations the pressure, temperature, and burning speed data are trimmed at the onset of cellularity as discussed in section 4.2. Lastly when φ=5.0 it is apparent that the flame is once again fully laminar and pressure data is considered until the flame reaches the wall.

Figure 14 presents a very different case for T_i=380, p_i=2.0atm, and φ=2.0. During this test by frame 7 there is already extensive cracking and disfiguration of the flame prior to it reaching a radius of 4cm. This means that the flame is fully cellular and cannot be considered in our model for laminar burning speed calculations because the area of the flame is required and with a non-spherical surface, the area cannot be calculated reliably.

4.2 Stretch

Flame stretch is the variation of flame area over time and can affect the calculated burning speed values by returning inflated values of burning speed. To circumvent stretch effects it is typical to

only consider flames with radii greater than 4cm, as conventionally it is agreed that stretch effects become negligible past this point [20-22]. Equation 7 presents the empirical definition of flame stretch where k is the stretch rate, A is surface area of the flame, t is the time since the inception of combustion, and r is the flame radius.

$$k = \frac{1}{A}\left(\frac{dA}{dt}\right) = \frac{2}{r}\left(\frac{dr}{dt}\right) \qquad (7)$$

In order to study the effects of stretch a series of tests at T_i=298, 350 and 380K were conducted at equivalence ratios of 0.6 and 3 and pressures corresponding to the isentrope. By conducting several different tests along the same isentrope the burning speed could be determined with different stretch rates due to differing flame radii. Figures 15 and 16 show the variation of laminar burning speed vs. stretch rates at T=398 where the isentrope plots overlap. These figures illustrate that at lean fuel mixtures (phi=0.6) the stretch rate is about 18 (1/s) which is very low when compared to the rich mixture (phi=3.0) which has a stretch rate of about 170 (1/s). These stretch rates illustrate that at phi=0.6 the flame radius is significantly larger than the flame radius at phi=3.0, as flames with small radii have significantly larger stretch rates. In Figures 15 and 16 the horizontal lines are the average burning speed obtained for the tests plotted against the stretch rate. It is expected that as more data points are collected along these istentropes that the trend of the data would fit these lines closely. Even with the minimum of three points at Phi=0.6 it is clear that the data already fits a horizontal curve. For phi=3.0 more test points are required to verify this trend. With these plots it is fair to state that beyond a radius of 4cm the impact of stretch rate on our burning speed results does not have a significant impact on our data.

4.3 Conditions Tested

Burning speed tests were conducted for syngas mixtures consisting of a 10:90 hydrogen to carbon monoxide ratio. The tests were conducted at initial temperatures of T_i=298 and T_i=380 with initial

pressures (P_i) of 0.5, 1, and 2 atmospheres which allowed the group to obtain burning speed results for temperatures ranging from 310 K to 520 K and over pressures from 0.5 atm to around 3 atm. Additionally at each of these initial conditions the following equivalence ratios were tested; φ=0.6, 1, 2, 3, and 5. Equivalence ratio is defined in equation 8, where (m_f/m_a) is the mixture ratio of fuel to air, and $(m_f/m_a)_{st}$ is the ratio of fuel to air required for stoichiometric combustion.

$$\phi = \frac{\frac{m_f}{m_a}}{\left(\frac{m_f}{m_a}\right)_{st}} \qquad (8)$$

4.4 Data Processing

As discussed in section 4.1 the laminar burning speed calculations were limited to flames with radii larger than 4 cm where the effects of stretch become negligible. Thus once a data file containing pressure time data over the duration of the combustion event was produced it was trimmed and the data obtained before the flame radius reached 4 cm and data that was obtained after the flame hit the wall was removed. The point at which the flame hits the wall is determined using the high speed camera and analyzing the combustion event on a frame by frame basis. Another method for determining when the flame reaches the wall is by inspection of the pressure time plots, an example is presented in Figure 17. In this plot there is a large spike in pressure, this spike in pressure indicates that the flame has reached the wall, thus all data after the pressure begins to rapidly increase must be discarded. After the trimming of the data it must be smoothed due to signal noise generated by high sample frequency in order to prevent the burning speed code from crashing. The overarching goal of this data smoothing is obtain data that reflects the physics of the combustion event. The data is smoothed using an exponential smoothing with a coefficient of 0.5, and is subsequently ordered in ascending form to satisfy the requirements of the thermodynamic

code. An example of raw versus smoothed pressure time data during the combustion event is presented in Figure 18.

4.5 Laminar Burning Speed Results

Experiments were conducted as each of the conditions listed in section 4.1 and the pressure time data from these experiments were fed into the thermodynamic code discussed in section 3. The laminar burning speed results generated by the thermodynamic code are presented in Figures 29 through 24. Figure 19 presents the burning speed data for T_i=298, P_i=0.5, and all tested equivalence ratios. From this graph it is clear that the leanest mixture, when phi=0.6, has the lowest laminar burning speed. As the equivalence ratio increases there is a rapid increase in laminar burning speed until the equivalence ratio is greater than 3. When phi=5.0 the mixture is too rich, and the burning speed is reduced. This exact trend can be seen through Figures 20 and 21 for the other initial pressures at room temperature. Between Figures 19-21, it is clear that as the pressure increases the laminar burning speed decreases. At higher pressures mixtures of equivalence ratios of 2 and 3 become unstable quicker than their more lean and rich (phi=0.6 and 5) counterparts respectively. In Figure 21 there are only two trends presented due to flame instability, the flames became cellular before the radii reached 4cm as discussed in section 4.1.

Figure 22 contains the burning speed data obtained for T_i=380, P_i=0.5, and all equivalence ratios tested. By inspection it is again clear that the lowest burning speed is achieved when phi=0.6, and as the equivalence ratio increases the burning speed also increases sharply until phi=3.0. Continually increasing the equivalence ratio beyond phi=3.0 yields a decrease in laminar burning speeds as the mixture becomes too rich. The trend of increasing burning speed with equivalence ratio until it is greater than three is seen in Figure 22, but not 23 due to flame cellularity.

As discussed for T_i=298 the trend of increasing instability and decreased burning speed is even more evident in Figures 22-24 where the three pressures tested with T_i=380 are presented. When the initial pressure of the mixture was P_i=2.0 in Figure 24 the only flame that did not experience instantaneous cellularity was the very rich phi=5.0 mixture. Additionally between these two sets of plots the strong impact of temperature is apparent, with an increased temperature the burning speeds are significantly higher than the same mixtures at room temperature.

4.6 Comparison with Previous Work

The results of laminar burning speed obtained during experimentation were compared with previous researchers at atmospheric temperature and pressure: where the most prevalent testing has been conducted. The comparison can be found in Figure 25, by inspection you can see that by in large our results were in agreement with literature for equivalence ratios of 0.6, 1 and 5, yet our data was inflated for equivalence ratios of 2 and 3 at atmospheric conditions.

5 Conclusions and Future Work

Laminar burning speeds of H_2/CO/Air mixtures with a H_2:CO ratio of 0.1:0.9 were determined over a range of temperatures between 298 K and 520 K over pressure range of 0.5 to 3 atmospheres, and equivalence ratios ranging from 0.6 to 5. It was observed that as the initial pressure of the mixture increases as does the instability of the flame. At initial pressures of 2 atm at both studied temperatures only very lean (φ =0.6) and very rich mixture (φ=5.0) flames were fully stable. The results for atmospheric testing were compared with preexisting literature and the results were acceptable within error.

5.1 Future Work

A) The overall quality of the data could be significantly improved at non atmospheric temperatures by redesigning the system in such a way that the temperature of the gases within the chamber can be determined in real time. Specifically in such a way that the thermocouple does not cause flame instabilities while positioned in a location that will allow the thermocouple to read the gas temperature not the wall temperature.

B) Additionally the heating system of the cylindrical chamber should be reconsidered either through the use of PID controllers in conjunction with the current band heaters or some sort of encasement heater as it is pivotal to the filling process that the temperature of the chamber is as near to stable as possible to avoid any filling errors due to thermally expanding or contracting gasses.

6 Appendices

6.1 Figures

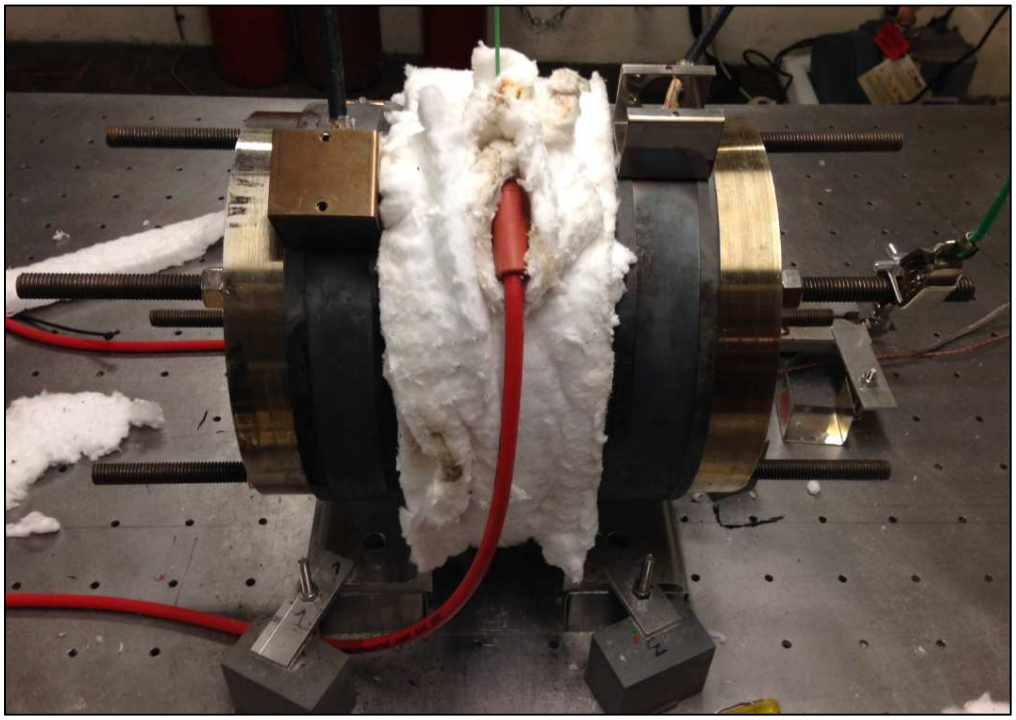

Figure 1: Cylindrical Chamber Profile

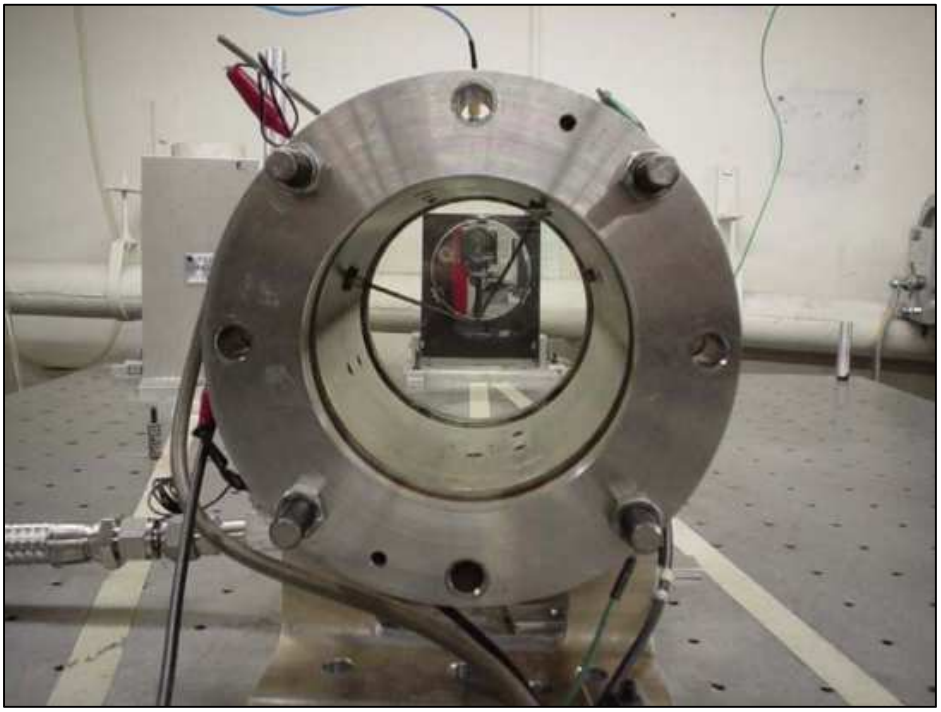

Figure 2: Cylindrical Chamber Face

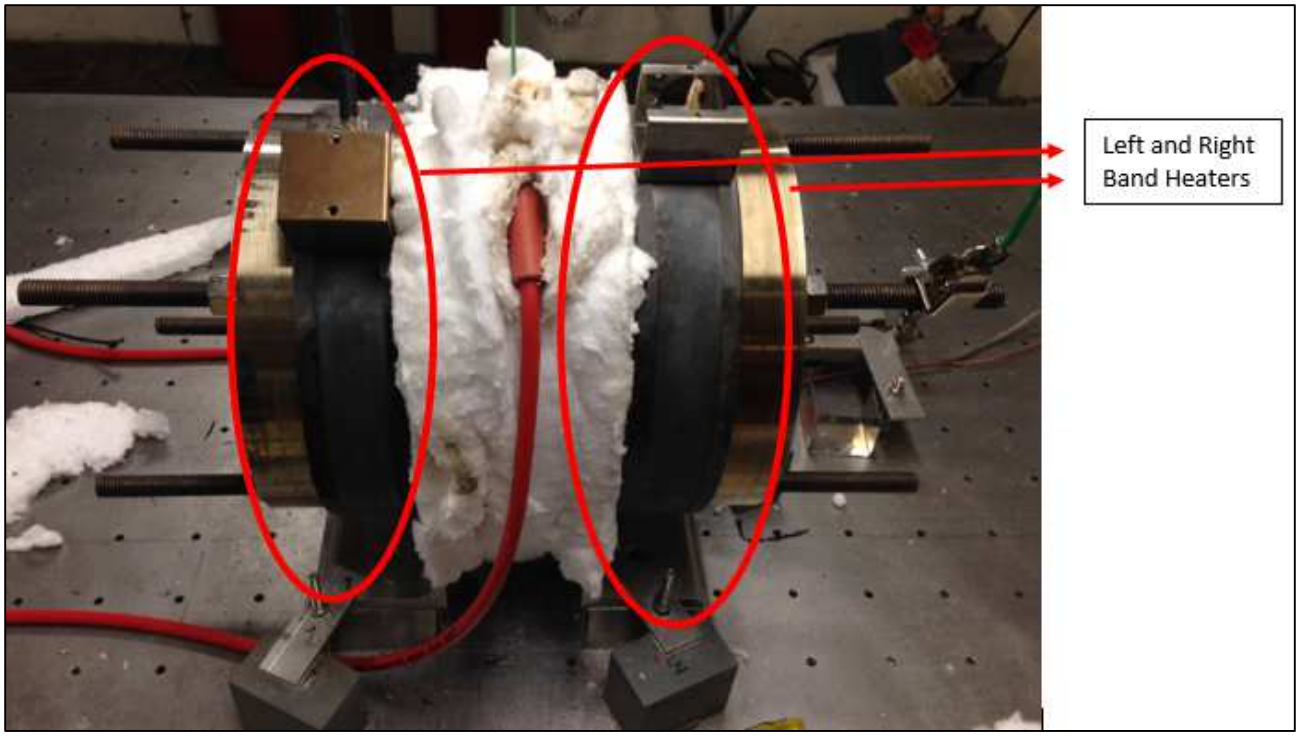

Figure 3: Band Heaters

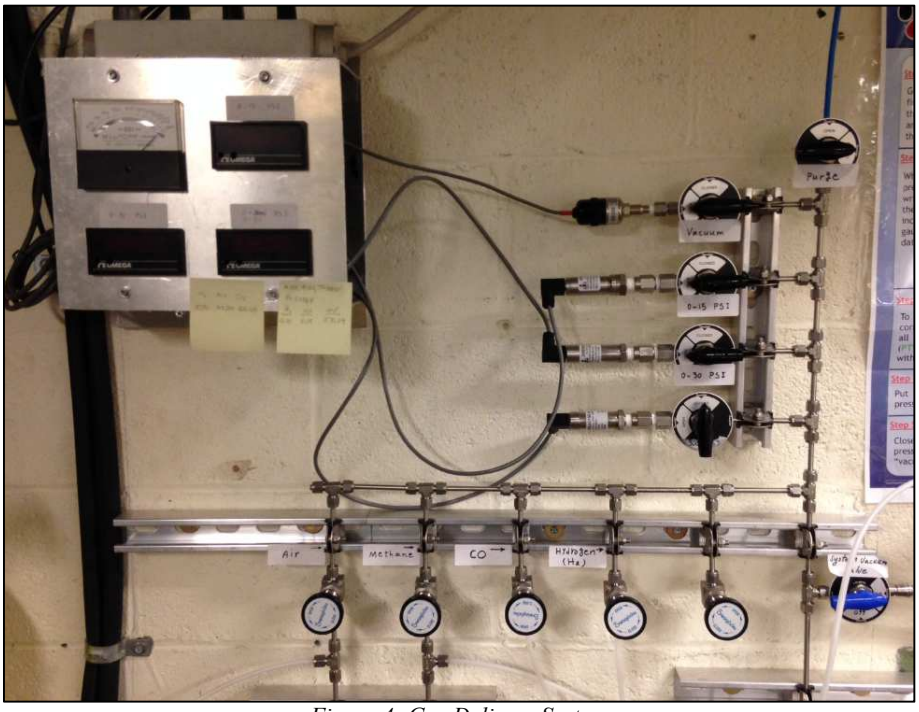

Figure 4: Gas Delivery System

Figure 5: Pressure Gauges

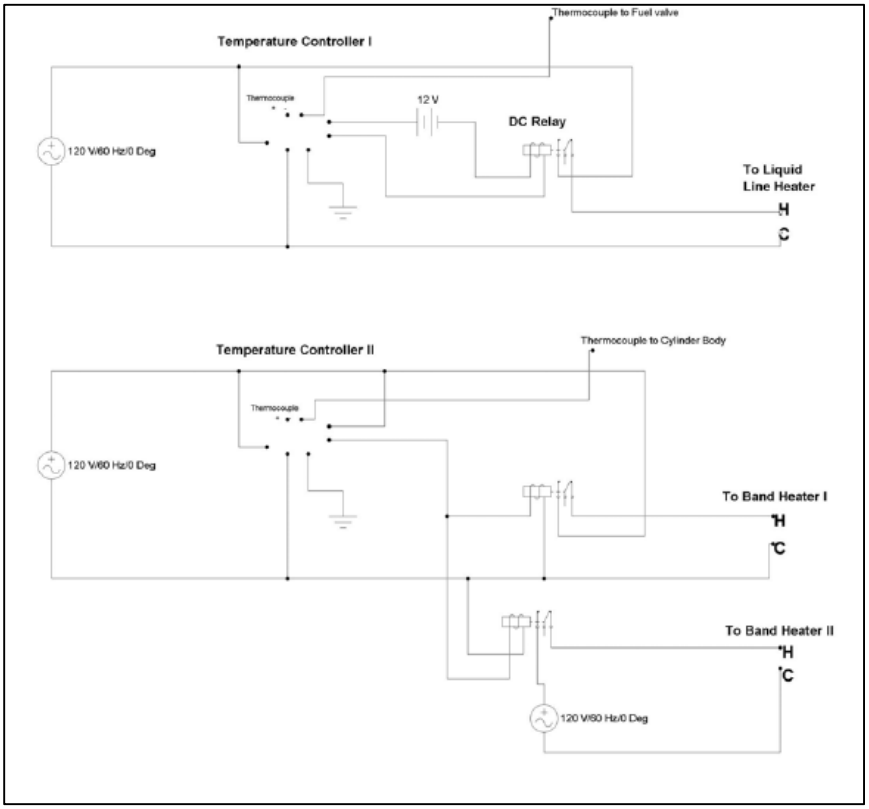

Figure 6: Electrical Schematic for Heating System

Figure 7: DP -7000 Controllers for Heaters

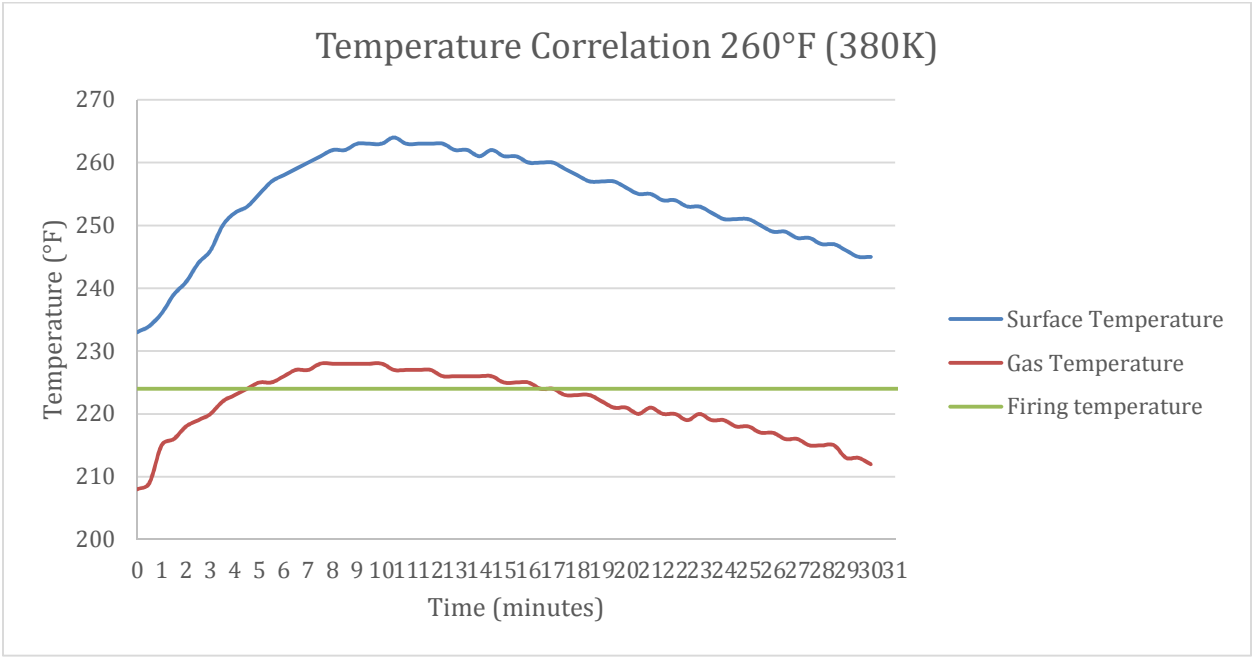

Figure 8: Temperature Correlation Plot

Figure 9: Extended Length Spark Plugs

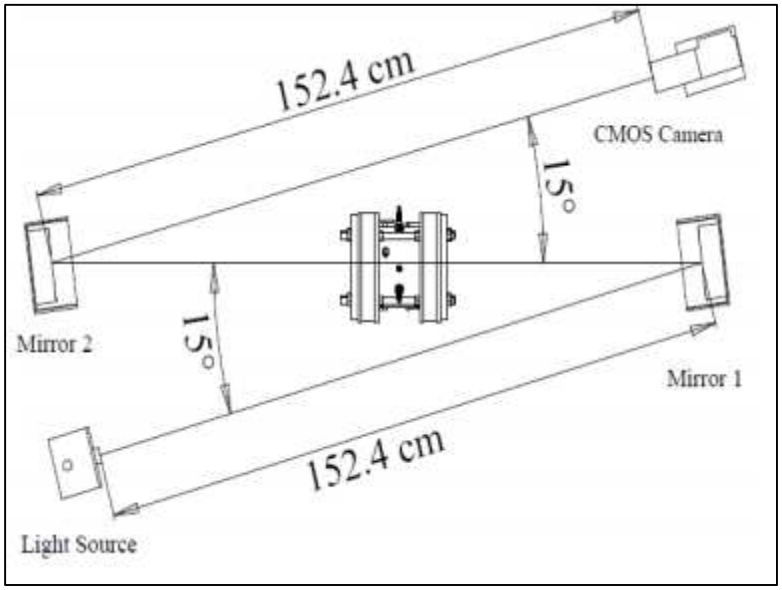

Figure 10: Shadow Graph System Schematic

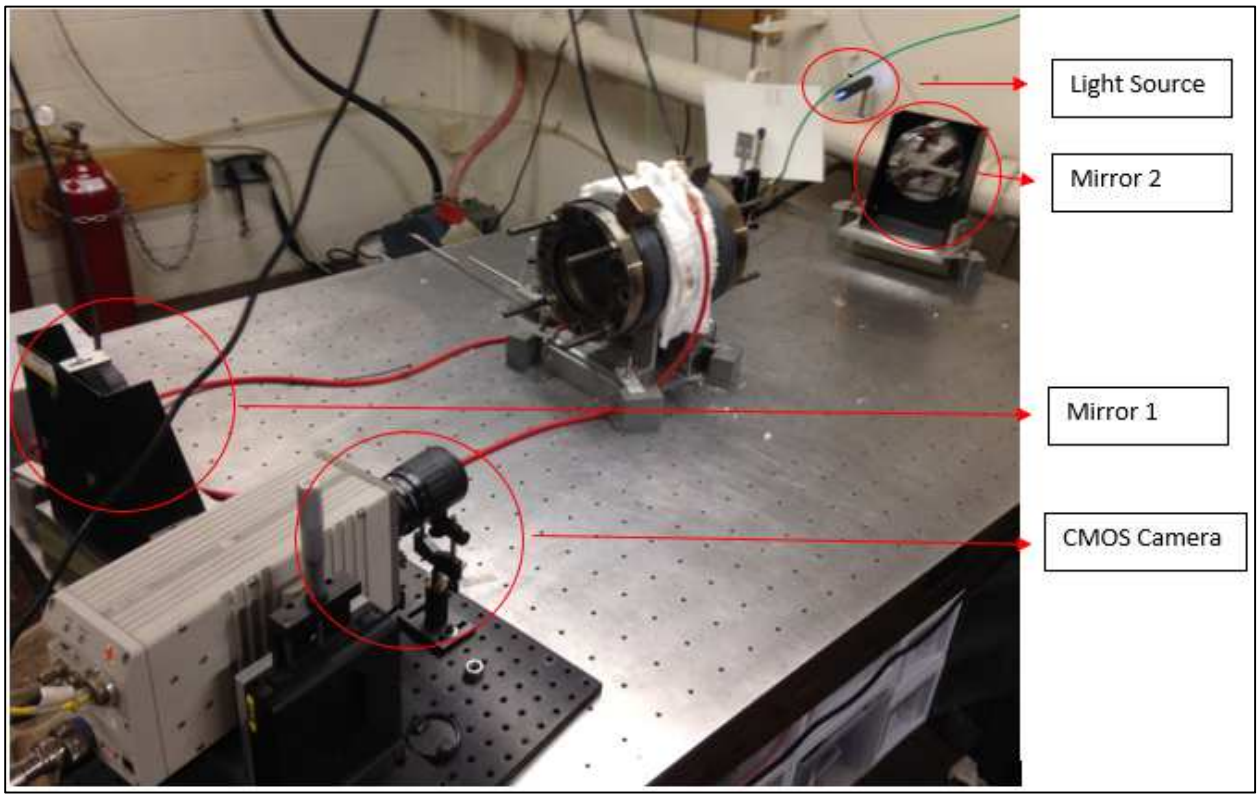

Figure 11: Shadow Graph System Lab Setup

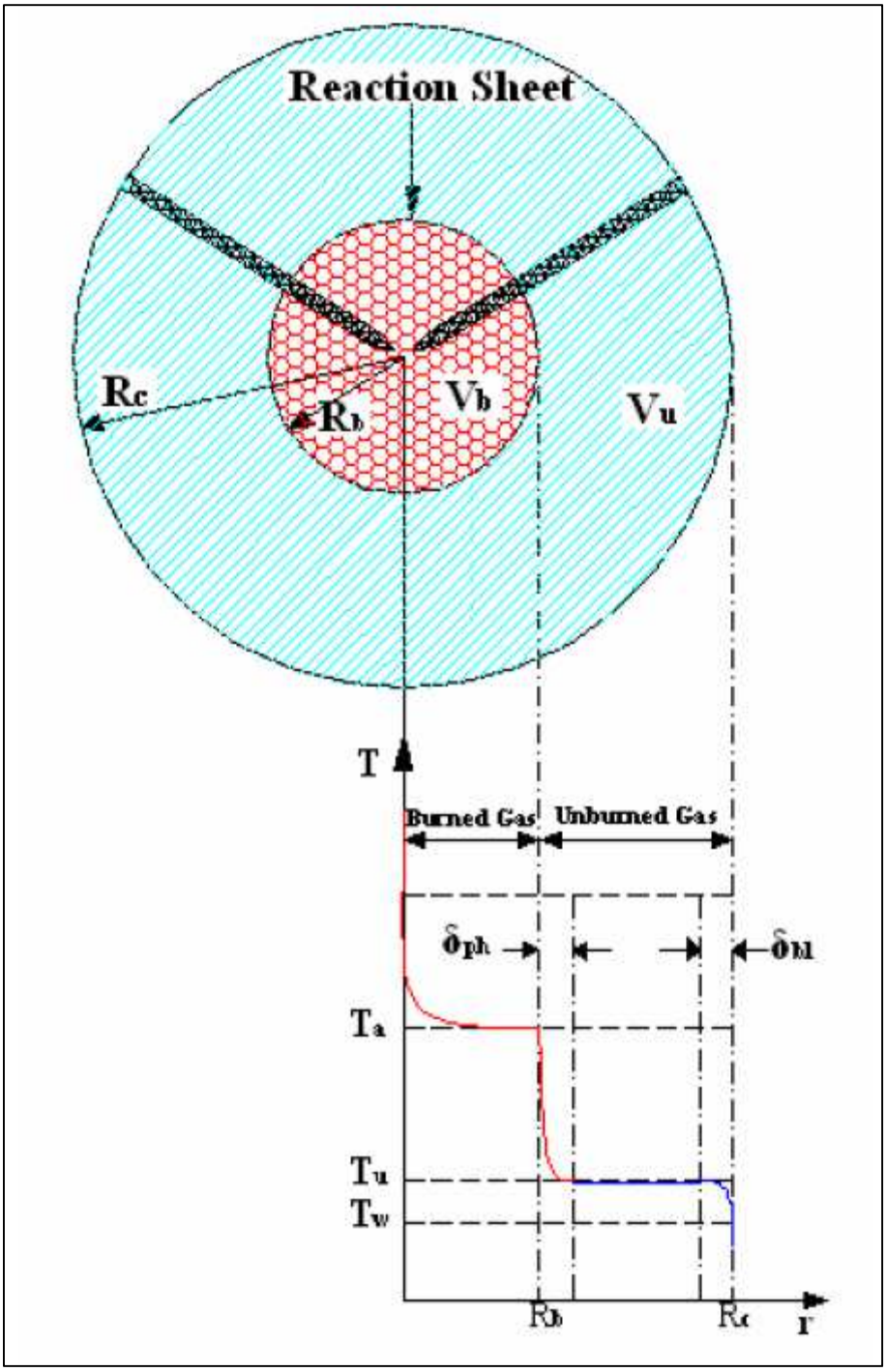

Figure 12: Diagram of Separate States of Gas During Combustion

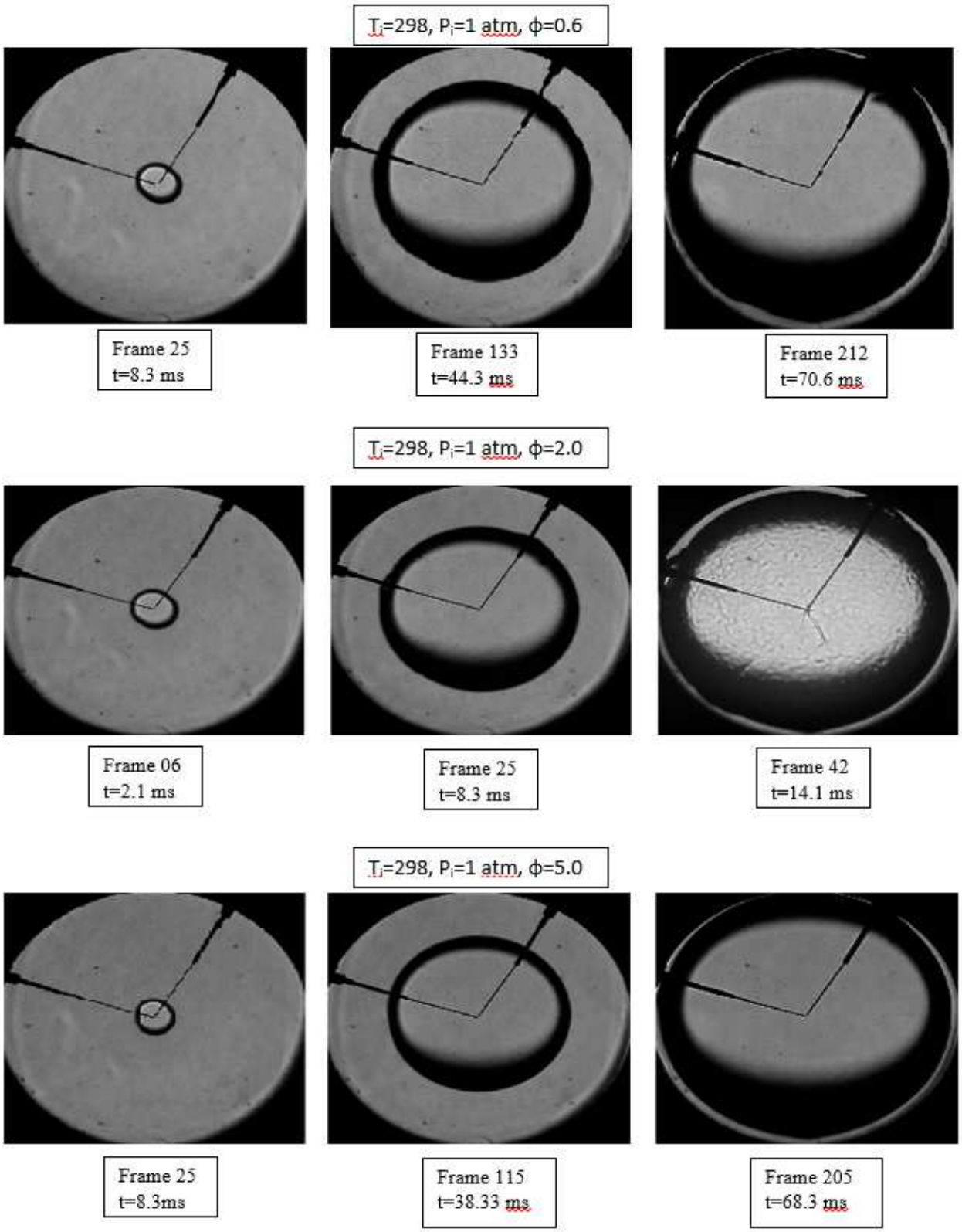

Figure 13: Flame Stability at Initial Temperature, Pressure, and 3 Equivalence Ratios

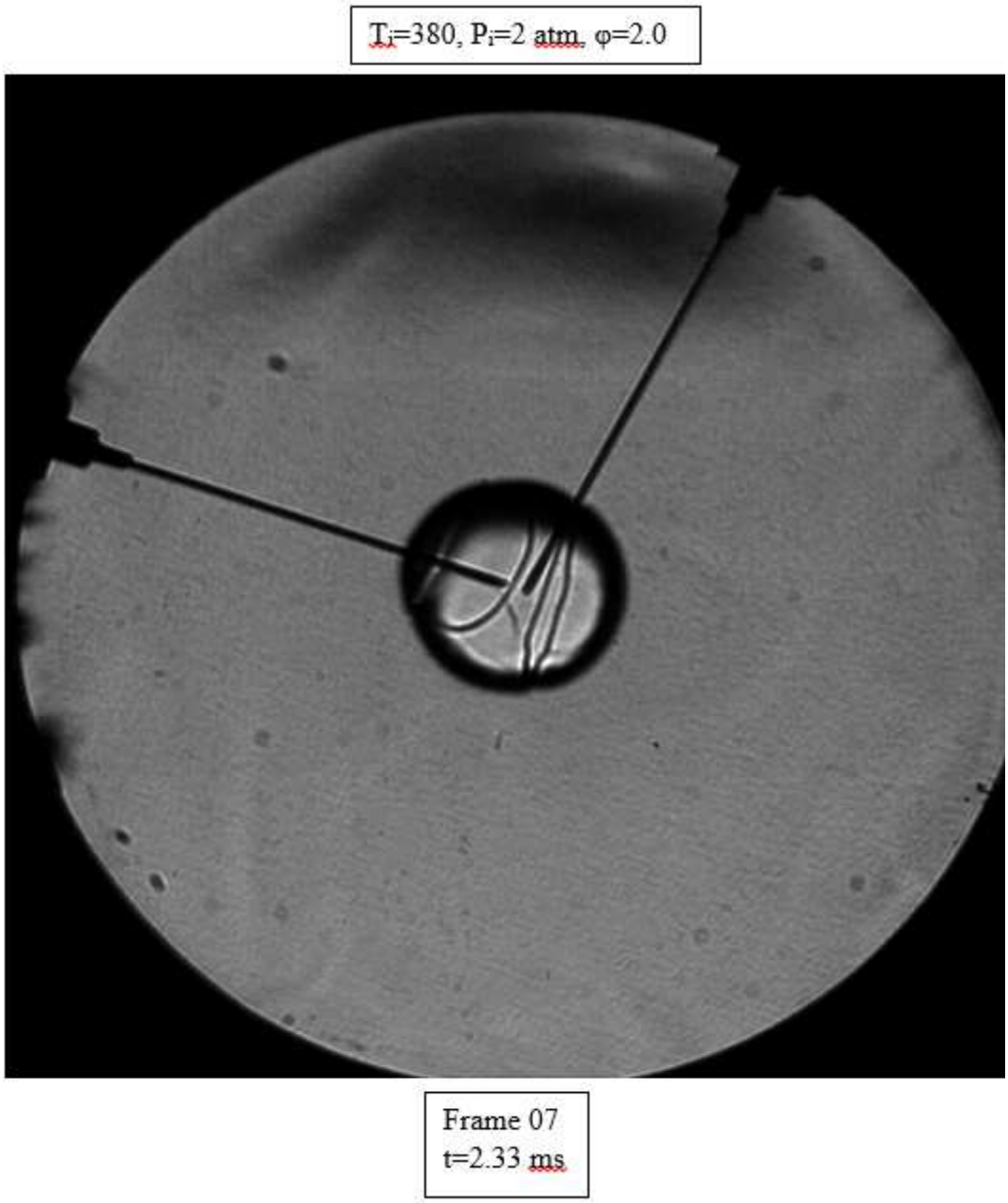

Figure 14: Fully Cellular flame prior to radius=4cm

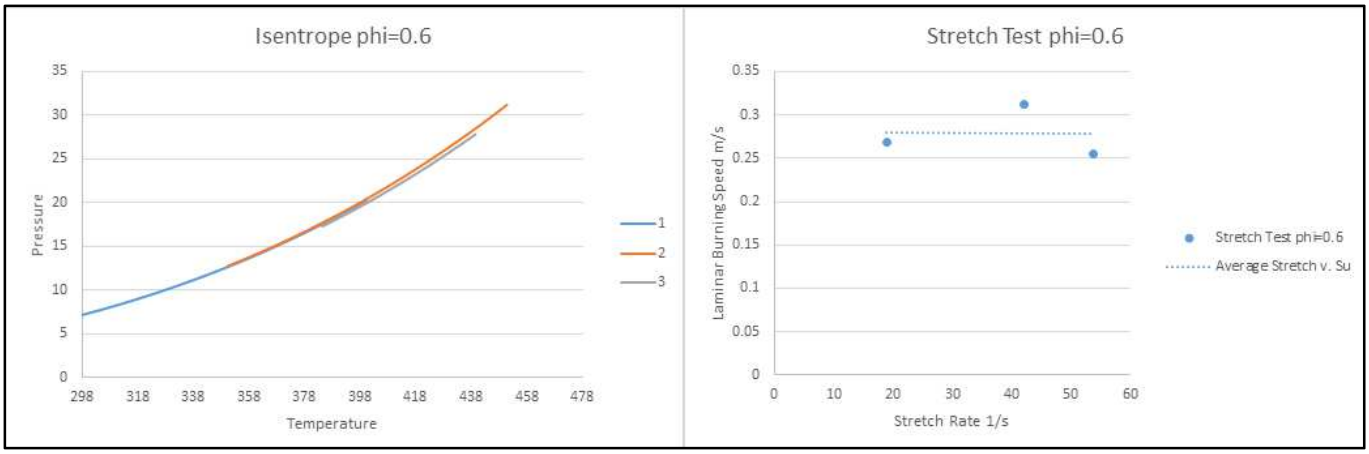

Figure 15(L) Phi=0.6 isentrope plot for Ti=298, 350, and 380 K (R): Phi=0.6 Laminar Burning Speed vs. Stretch for Ti=298, 350, and 380K

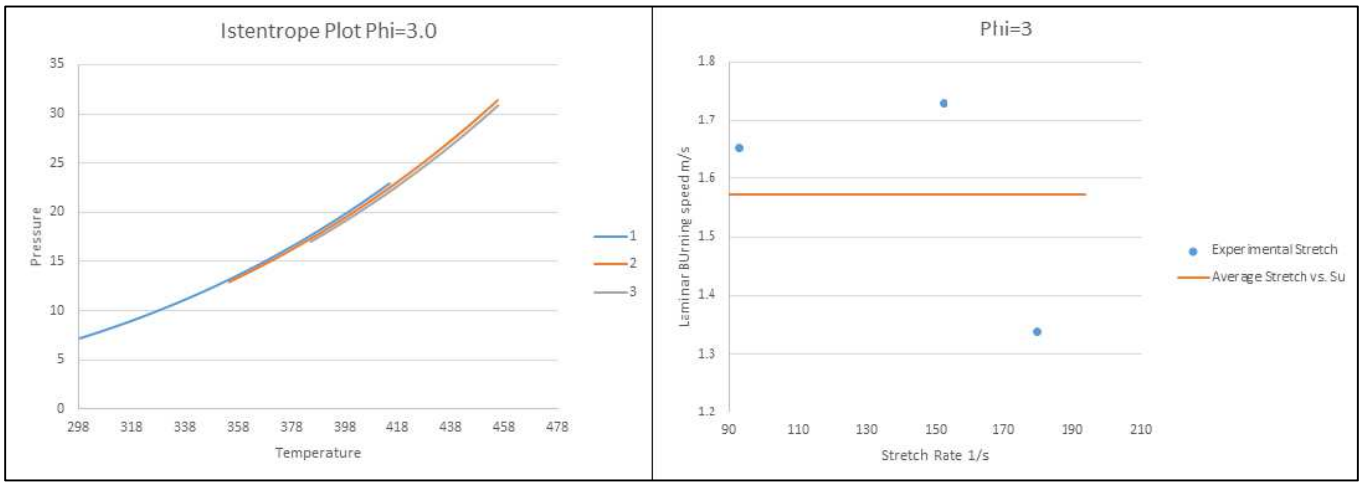

Figure 16: Phi=3.0 isentrope plot for Ti =298, 350, and 380 K (R): Phi=3.0 Laminar Burning Speed vs. Stretch for Ti =298, 350

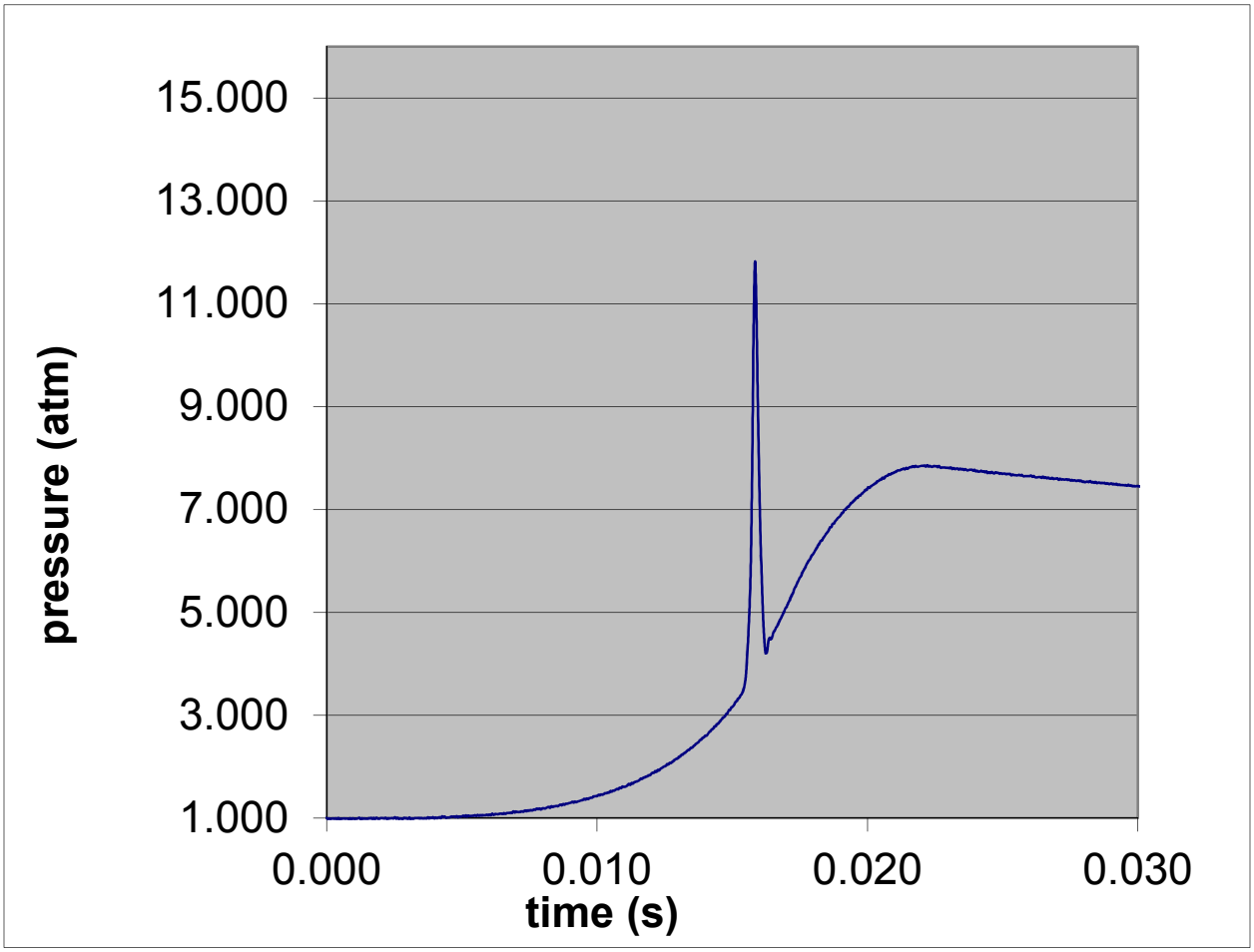

Figure 17: Pressure Time Experimental Data

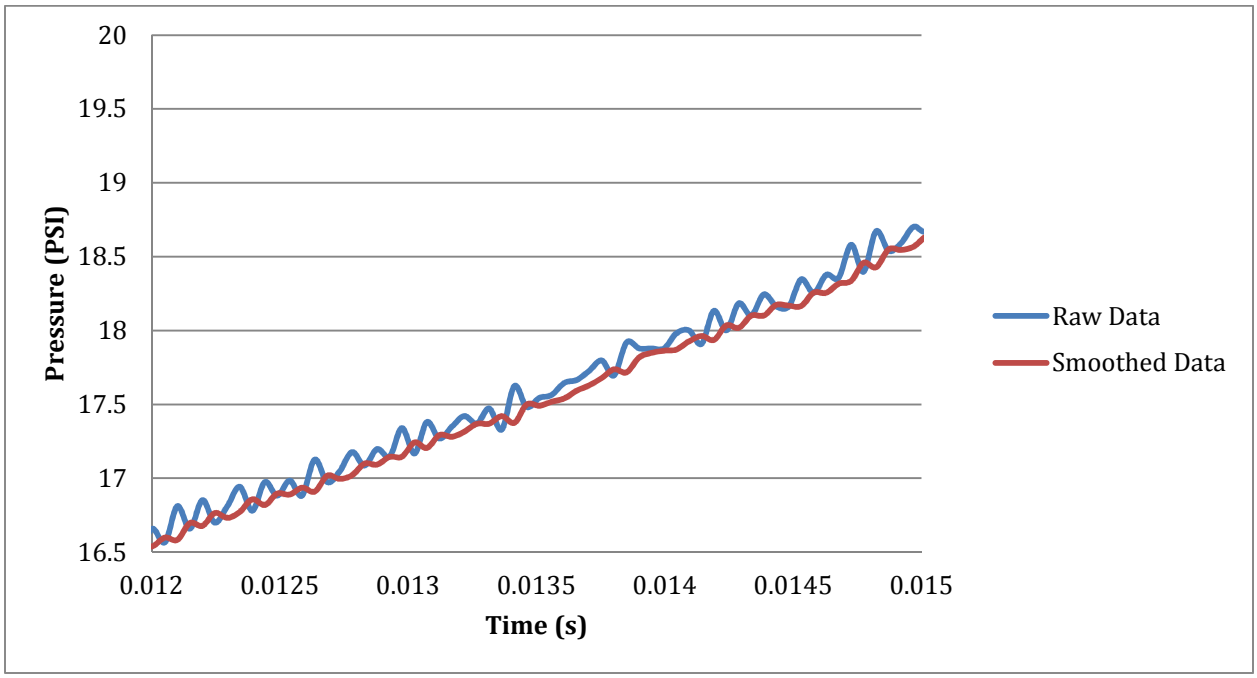

Figure 18: Raw Pressure v. Time data compared to processed 'smooth' data

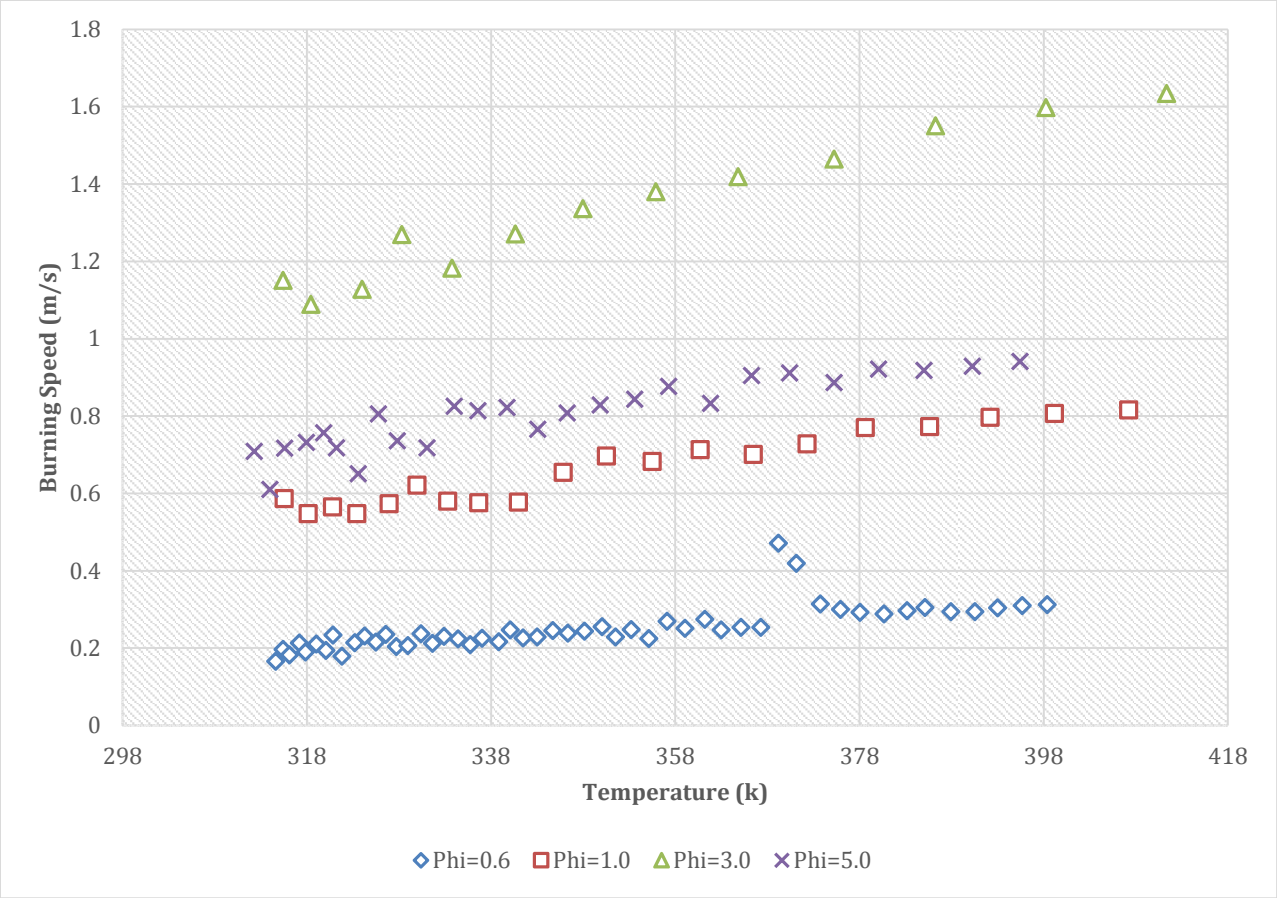

Figure 19: Laminar Burning Speed vs. Temperature T_i = 298 P_i=0.5atm

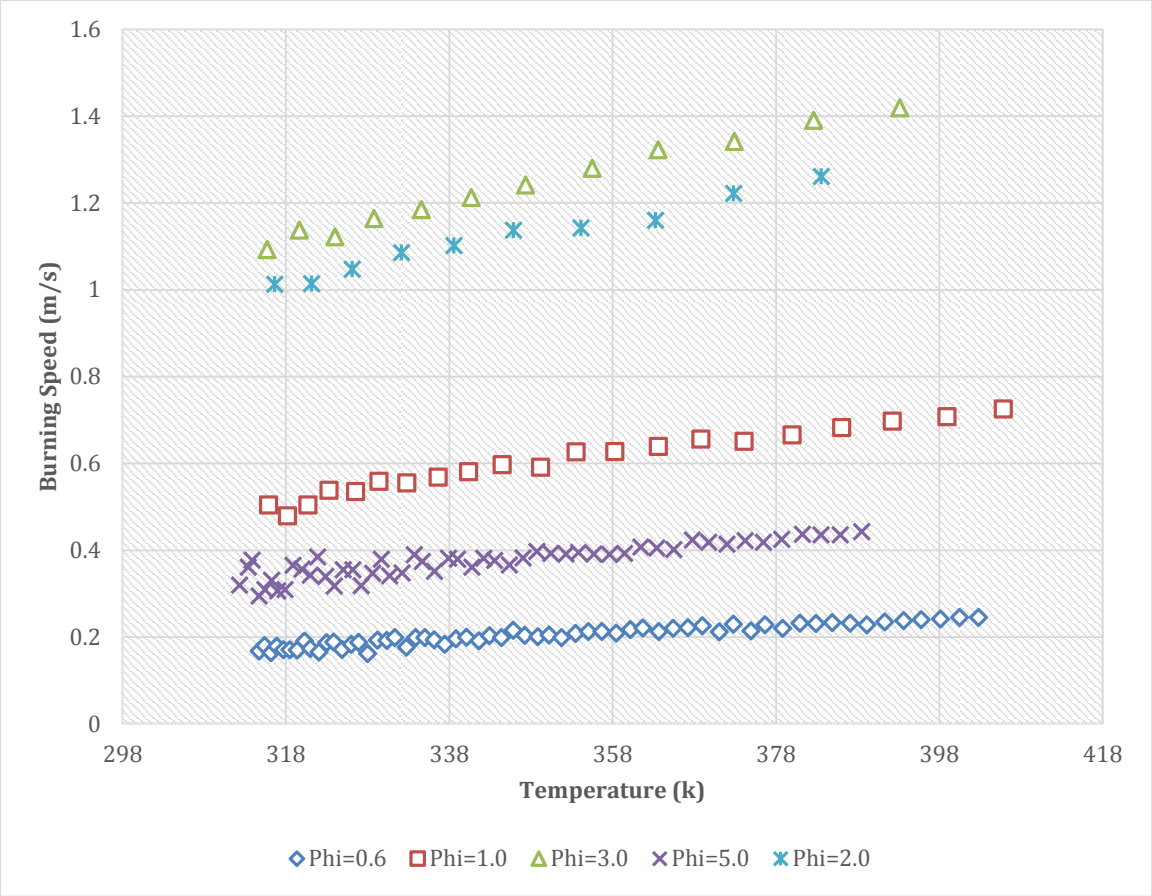

Figure 20: Laminar Burning Speed vs. Temperature T_i = 298 P_i=1.0atm

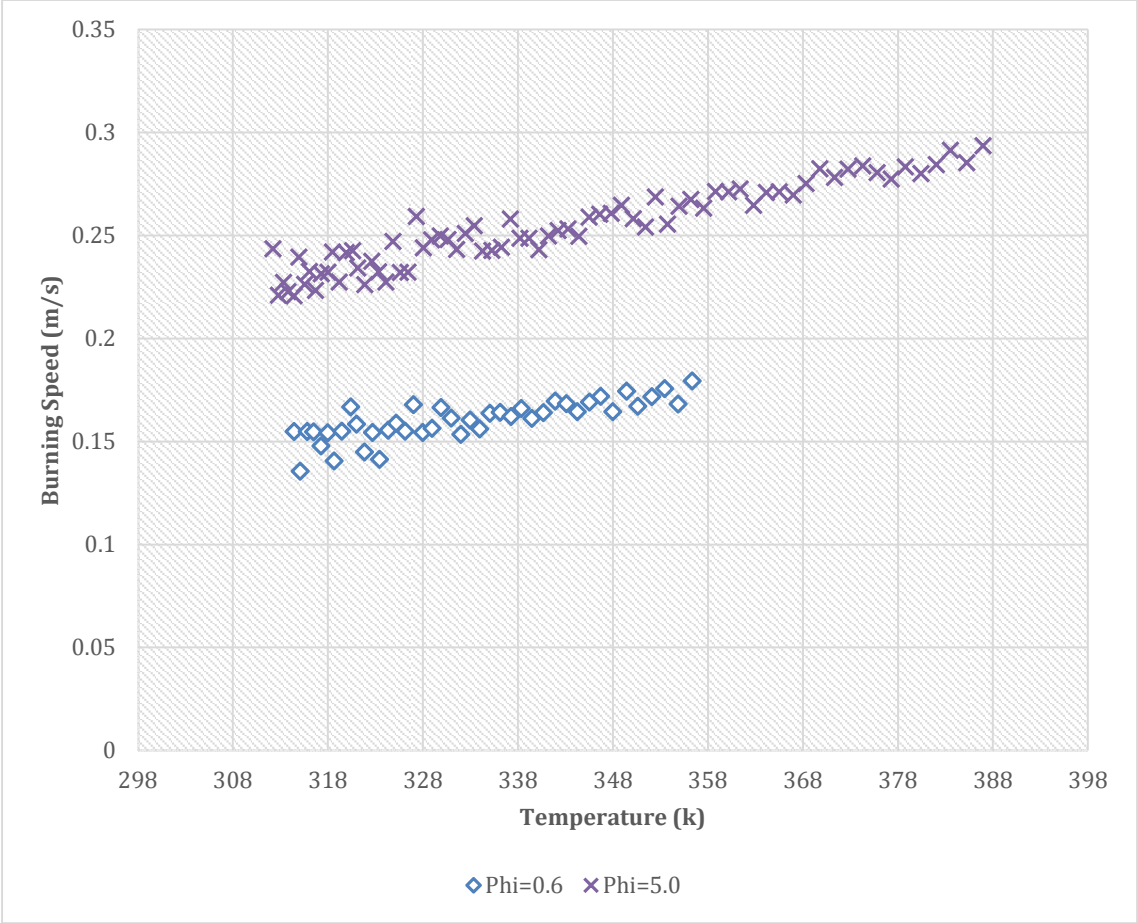

Figure 21: Laminar Burning Speed vs. Temperature T_i = 298 P_i=2.0atm

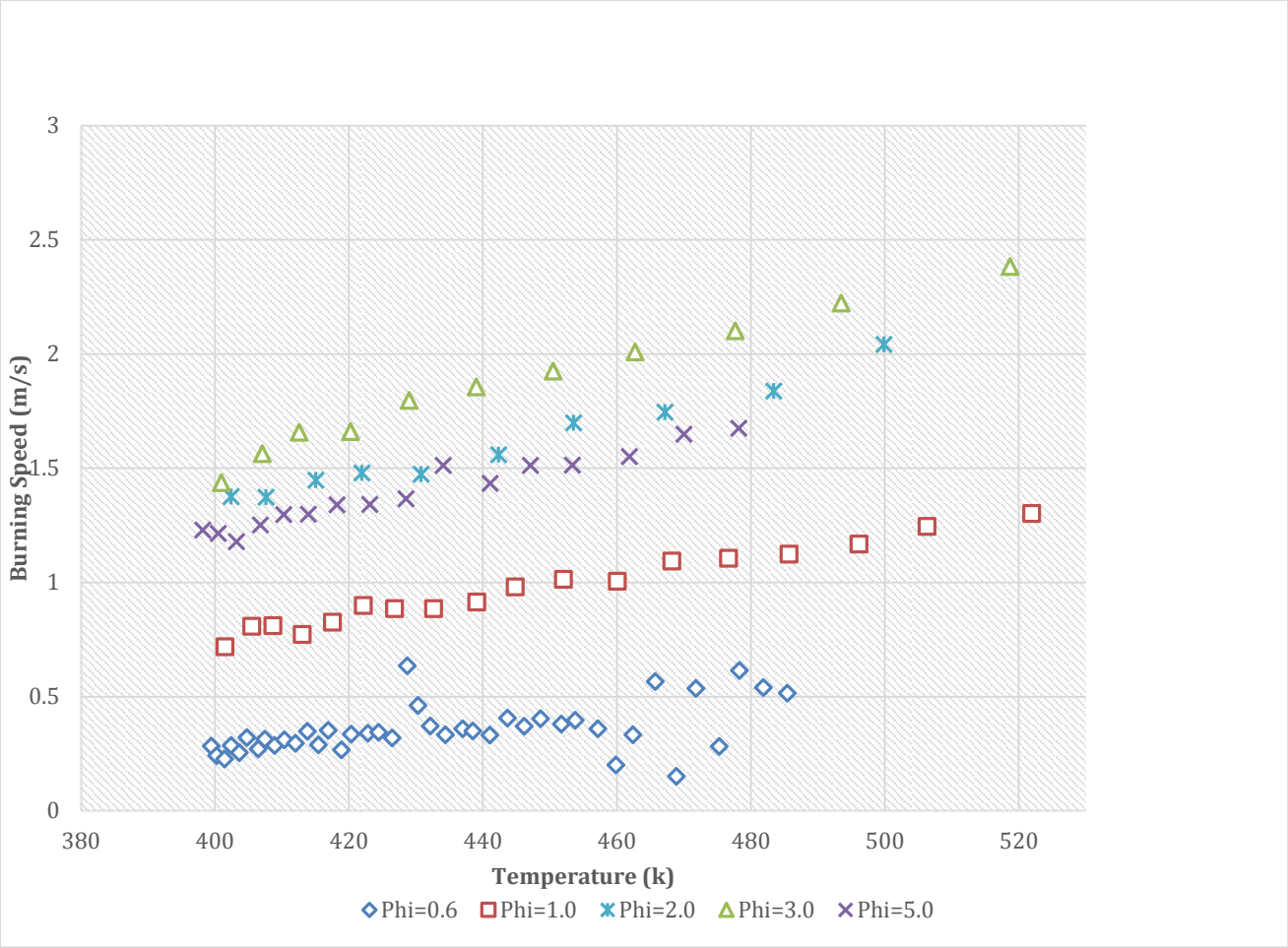

Figure 22: Laminar Burning Speed vs. Temperature T_i = 380 P_i=0.5 atm

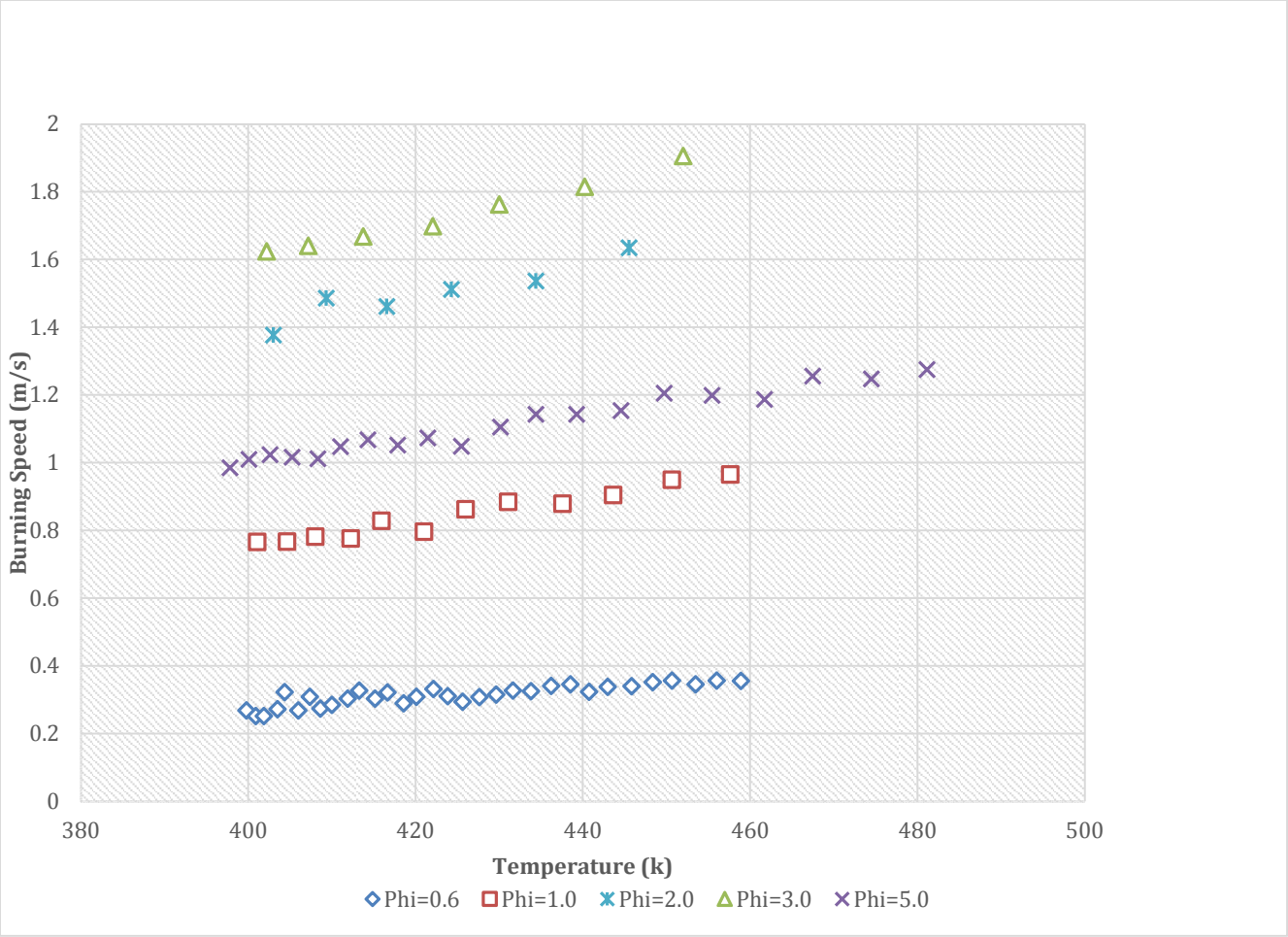

Figure 23: Laminar Burning Speed vs. Temperature T_i = 380 P_i=1.0 atm

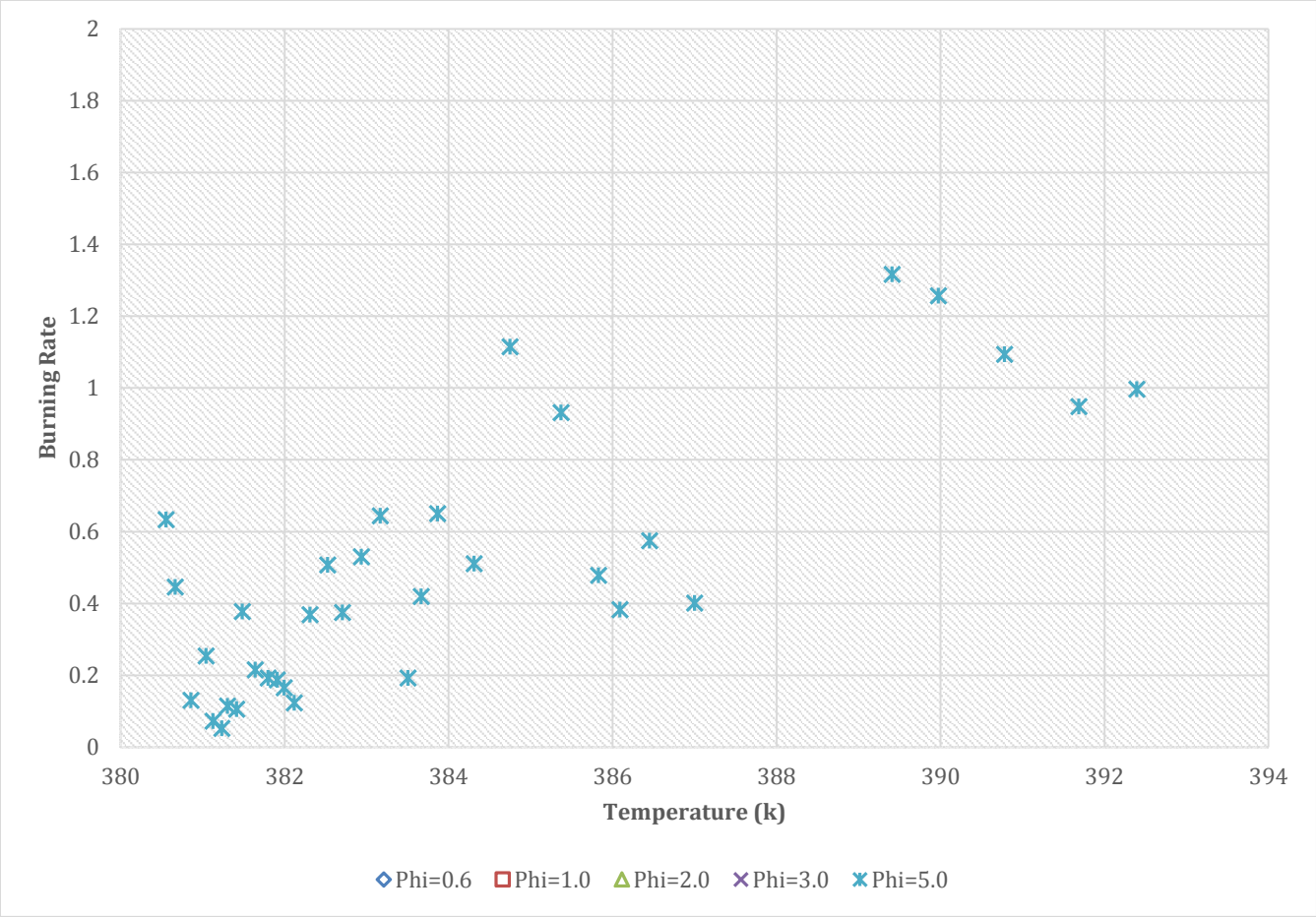

Figure 24: Laminar Burning Speed vs. Temperature T_i= 380 P_i=2.0 atm

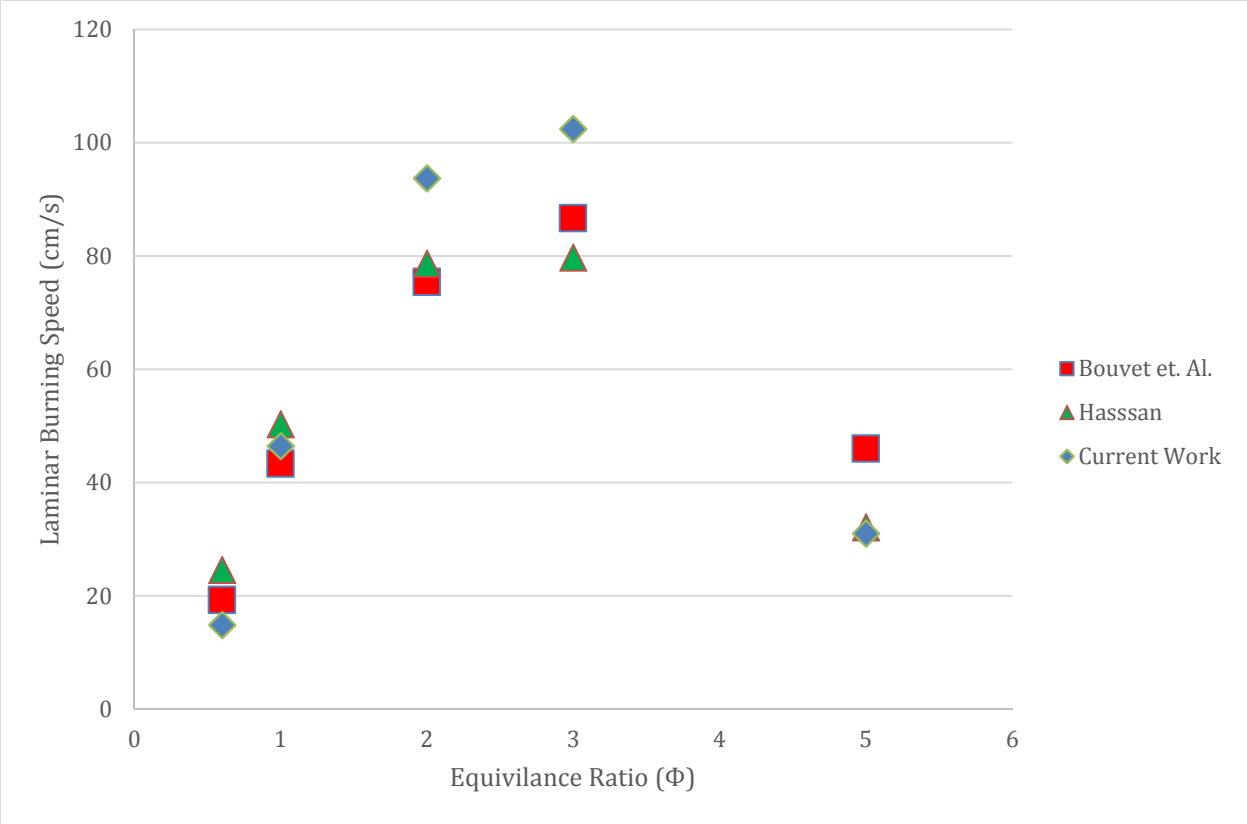

Figure 25: Comparison with literature at atmospheric pressure, To=298 and various equivalence ratios

6.2 Tables

Chamber Surface Temperature (K)	Internal Gas Temperature (K)
361	350
402	380
526	480

Table 1: Gas Temperature Correlation

7 References

1. Keck, J. C., *Turbulent Flame Structure and Speed in Spark Ignition Engines*, Nineteenth International Symposium on Combustion, 1982, 1451-1466

2. Ferguson, C. R. and Keck, J. C., *On Laminar Flame Quenching and Its Application to Spark Ignition Engines*, Combustion and Flame, 28-2 (1977), 197-205

3. Frenklach, M., *Reduction of Chemical Reaction Models, Numerical Approaches to Combustion Modeling*, Progress in Astronautics and Aeronautics, 1991,135, Chater 5, 129-150
4. Linnett, J. W., *Methods of Measuring Burning Velocities*, Fourth Symposium (International) on Combustion. 1953. Baltimore: Williams and Wilkins
5. Andrews, G. E. and Bradley D., *Determination of Burning Velocities: A Critical Review,* Combustion and Flame, 18 (1972), 133-153

6. Rallis C. J. and Garforth A. M., *Determination of Laminar Burning Velocity,* Progress in Energy and Combustion Science, 6 (1980) 303-329
7. Van Maaren, A, Thung, D.S., De Goey, L.P.H. (1994). *Measurement of Flame Temperature and Adiabatic Burning Velocity of Methane/Air Mixtures*. Combust. Sci. and Tech. 96, 327-344.
8. Linteris, G.T. *Burning Velocity of 1,1-difluroethane* (R-152a), ASHRAE Transactions.
9. Wu, C.K., Law, C.K. (1984). *On The Determination of Laminar Flame Speeds From Stretched Flames. The Combustion Institute*. 1941-1949
10. Egolfopoulos, F.N., Cho, P., Law, C.K. (1989). *Laminar flame speeds of methane air mixtures under reduced and elevated pressures*. Combustion and Flame. 76, 375-391.
11. Andrews, G.E., Bradley, D. (1972). *Determination of Burning Velocities: A Critical Review. Combustion and Flame*. 18, 133-153
12. Eisazadeh-Far, K., Parsinejad, F., Metghalchi, H. (2010). *Flame structure and laminar burning speeds of JP-8/air premixed mixtures at high temperatures and pressures*. Fuel. 89, 1041-1049
13. Takizawa, K., Takahashi, A., Tokuhashi, K., Kondo, S., Sekiya A. (2005). *Burning velocity measurement of fluorinated compounds by the spherical-vessel method*. Combustion and Flame. 141, 298-307.
14. Lewis, B., von Elbe, G. (1961*). Combustion, Flames, and Explosion of gases*, 2nd edition, Academic Press.
15. Metghalchi, H., Keck, J.C. (1980). *Laminar Burning Velocity of Propane-Air Mixtures at High Temperature and Pressure. Combustion and Flame*. 38, 143-154.
16. Natarajan, J., Lieuwen, T., and Seitzman, J., 2007, *Laminar flame speeds of H2/CO mixtures: Effect of CO2 dilution, preheat temperature, and pressure*, Combust. Flame, 151, pp. 104–119.
17. Sun, H., Yang, S. I., Jomaas, G., and Law, C. K., 2007, *High-pressure laminar flame speeds and kinetic modeling of carbon monoxide / hydrogen combustion* 31, pp. 439– 446.
18. Som, S., Ramírez, a. I., Hagerdorn, J., Saveliev, a., and Aggarwal, S. K., 2008, *A numerical and experimental study of counter flow syngas flames at different pressures* Fuel, 87, pp. 319–334.

19. Natarajan, J., Kochar, Y., Lieuwen, T., and Seitzman, J., 2009, *Pressure and preheat dependence of laminar flame speeds of H 2/CO/CO2/O2/He mixtures*, Proc. Combust. Inst., 32 I(1), pp. 1261–1268.
20. Casey Bennett, 2011, *Laminar Burning Speed and Flame Structure of 1,1-Difluoroethane (HFC-152A)/Air and Difluoromethane (HFC-32)/Air Mixtures*. Northeastern University
21. A. Moghaddas, K. Eisazadeh-Far, H. Metghalchi, *Combust Flame* 159 (2012) 1437–1443.
22. Ali Moghaddas, Casey Bennett, Emad Rokni, Hameed Metghalchi, *HVAC&R Research*, Jan2014